

Dissipated Energy Measurements of Metal Material during High-cycle Fatigue Test Process

Yuan LI^{*,a,b}, Francois MAQUIN^c, Zhicheng LIU^a, Chao JIANG^a, Xu HAN^a

^aState Key Laboratory of Advanced Design and Manufacturing for Vehicle Body, College of Mechanical and Vehicle Engineering, Hunan University, Changsha, 410082, China

^bDepartment of Traffic and Transportation Engineering, College of Basic Education for Commanding Officers, National University of Defense and Technology, Changsha, 410003, China

^cLaboratoire de Mecanique et Procedes de Fabrication(LMPF), Arts et Metiers ParisTech, BP 508 Rue St Dominique, Chalons-en-Champagne, 51006, France

Abstract

In this paper, the high-cycle fatigue characterization of 316L stainless steel was studied based on dissipated energy measurement. At first, the dissipated energy per cycle was deduced from temperature field of specimen surface using an experimental mechanical method. Then, variations of dissipation energy per cycle were in-situ monitored during each high-cycle fatigue test under different stress levels. The results show that dissipated energy is mainly constant after the initial 5% cycles of total fatigue lifetime. Dissipated energy versus fatigue lifetime fitting curve shows the same pattern as the traditional stress versus fatigue lifetime curve.

Key words: Dissipated energy, metal material, high-cycle fatigue, fatigue lifetime

1. Introduction

High-cycle fatigue characterization of metal material is a time consuming and expensive statistical process. Thus, various theories and alternative accelerated methods to estimate fatigue characteristics have been of great interest at home and abroad [1] over a number of years. From an energy point of view, under the repeated mechanical energy input provided by the loading, dislocation are created and rearranged into the specific micro-structures. These micro-structural modifications accompanied with heat dissipation energy, lead to progressive energy storage.

By observing the local temperature rise, many authors developed many accelerated methods to estimate fatigue limit or S-N curve, such as one curve method [2] and two curve method [3], Amiri method [4], quantitative thermographic method [5], self-heating method [6] et.al. Unfortunately, fatigue characteristics resulting from these approaches are questionable: the local temperature rise is correlated with heat-conduction, heat-convection and heat-exchange, and especially affected by the environment temperature fluctuation, and the physical reasons leading to these estimations are not yet well understood. A better understanding of the physical origin of dissipated energy is required to better interpret the local temperature rise. The relative dissipated energy was firstly deduced from local temperature

*Corresponding author: yuanli@nudt.edu.cn

rise using a two-dimensional convolution local heat conduction equation under fatigue loadings [7, 8]. Considering the environment temperature and the thermo-elastic effect, the accurate dissipated energy per cycle was achieved [9]. In this paper, a precise temperature measurement experiment program was developed to compute dissipated energy. The variation of dissipated energy per cycle was in-situ monitored during each high-cycle fatigue test process under different stress levels.

2. Theory and Experiment Set-up

To achieve the goal of this work, it is necessary to perform precise energy dissipation measurements in high cycle fatigue processing.

2.1. Materials

Stainless steel 316L is a low-carbon stainless austenitic steel. It's composed of 0.03 C, 2 Mn, 0.045 P, 0.03 S, 0.75 Si, 16-18 Cr, 0.01 N, 2-3 Mo, 10-14 Ni (in wt.%). The thermo-mechanical properties of 316L stainless steel are reported in Tab.1. The specimens were machined from a 3mm thick cold rolled sheet and machined in the rolling direction. Before the high cycle fatigue test, three tensile tests was performed to determine the 0.2% yield stress ($\sigma_{0.2\%} = 295MPa$) and ultimate tensile stress ($\sigma_b = 587MPa$).

Table 1: Thermo-mechanical and Mechanical properties(at 20 °C)

	ρ ($kg.m^{-3}$)	C ($J.kg^{-1}K^{-1}$)	k ($m^{-1}.K^{-1}$)	α ($10^{-6}.K^{-1}$)	E (GPa)	$\sigma_{0.2\%}$ (MPa)	σ_b (MPa)	Ref.
316L	7960	500	14	14.8	195	295	585	[10]

2.2. Dissipated energy measurements

The dissipative source d_1 of the material were computed from the surface temperature fields of the loaded specimen with a rectangular active gauge section (width $l=20mm$ and length $lu=30mm$). As the surface temperature variations with plastic strain are very small, precise temperature field measurements are required. A step-by-step mathematical description and details about the method performance are available in [9, 11].

A loaded sheet specimen and a dummy specimen were used to dissipated energy measurement. The dummy specimen localized next to the loaded specimen was made from the same material as the loaded one (Fig.1, left picture). It's used to monitor the environment temperature variation during the temperature filed acquisition. Both loaded and dummy specimens were coated with a thin layer of black paint to enhance their emissivity. To lower the environment noise, an insulation equipment was designed and placed around the specimen. Besides, a black curtain was surrounded to avoid external radiative reflections onto the specimens (Fig.1,right picture).

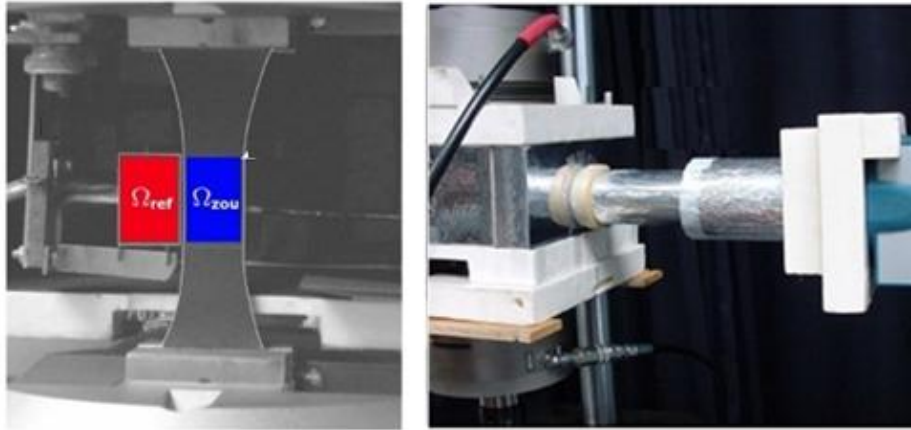


Figure 1: Specimens position (left) under fatigue machine and thermal insulation box (right).

Experiments under cyclic loading were conducted with a INSTRON 8801 axial servo-hydraulic load frame at room temperature. Each high cycle fatigue test was load-controlled. The temperature field of the observed Ω_{sp} and Ω_{dum} were measured using a 350Hz sampling and an integration time of 1200 μs infrared camera (CEDIP Jade MW) with a resolution of 160×120 pixels. The camera, which sensor is cooled down by a Rotary Stirling engine, was started about 4h before the tests in order to ensure its thermal stability. Moreover, the origin manufacturer calibration was used to ensure the precise dissipated energy measurement in this study. Fig.2 shows the dissipated energy E_{d1}^i obtained with and without the insulation calibration.

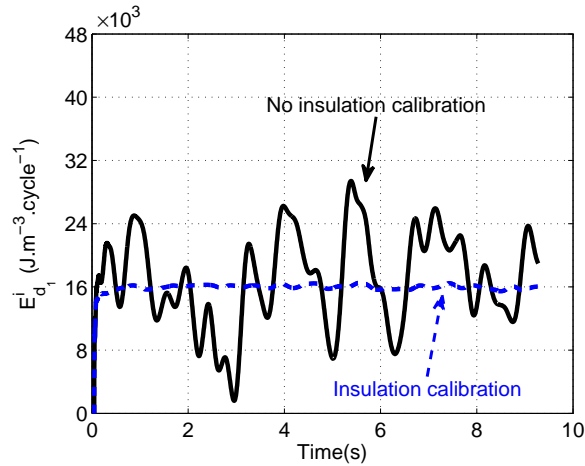


Figure 2: Evolution of dissipated energy difference with and without the insulation calibration.

During each test, the thermal fields of the observed areas Ω_{sp} and Ω_{dum} were stored for 20s (7000 images), which divided in two sequences (Fig.3):

-At the first 5s, the applied stress on the specimen was constant and equal to the mean stress σ_m . The mean stress being small compared to the material yield stress, creep and associated dissipated energy is negligible. Thus, during these 5s, the intrinsic dissipative sources d_1 of both specimen and dummy were assimilated to zero. The measured thermal drifts are due to the convection (loaded specimen and dummy) or conduction (loaded specimen) and represent the initial conditions.

-At the second 15s, the specimen was loaded with a stress such as $\sigma = \sigma_m + \sigma_a \cos(2\pi ft)$, where σ_a is the alternate stress amplitude and f is the loading frequency ($f=14\text{Hz}$). The temperature fields acquisition was from $t=5\text{s}$ and lasted 15s (210 cycles). The temperature field variations acquired due to the intrinsic thermo-mechanical sources. The alternative temperature variation are due to the thermo-elastic sources S_{th} (thermoelastic coupling effect) while the mean temperature increase is due to the dissipative sources d_1 .

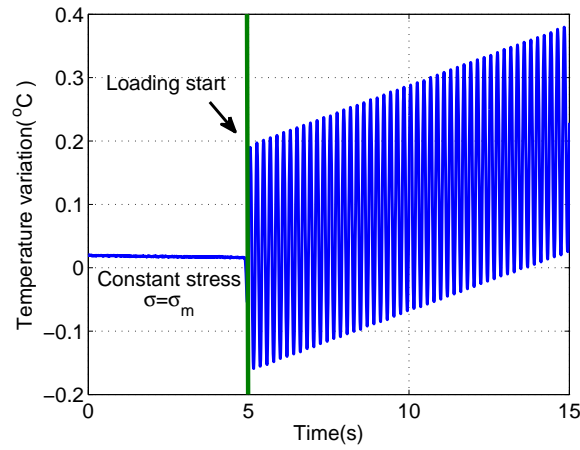


Figure 3: Temperature variation during a temperature field measurement under $R_\sigma=0.2$, $\sigma_{max}=380\text{MPa}$, 316L specimen.

The measured temperature fields were assumed to be representative of the material temperature through the specimen thickness, and the thermo-mechanical sources d_1 and S_{th} were estimated using the local energy balances equations. By combining the balance energy equations before and after the start of the the loading on both loaded specimen and dummy, the following energy balance equation was obtained:

$$\rho C \left(\frac{\partial \theta}{\partial t} - \left[\frac{\partial \theta}{\partial t} \right]_{t=0^-} \right) - k \Delta_2 \theta + \rho C \left(\frac{\theta}{\tau_{th}^{2D}} \right) = d_1 + S_{th} \quad (1)$$

where ρ is the material density, C is the calorific capacity, k is the thermal conductivity and Δ_2 is the Laplacian operator, θ is the local temperature variation of the specimen due to the thermo-mechanical sources. Eq.(1) underlines that these thermo-mechanical sources produce three major effects: a change in heat rate ($\rho C \left(\frac{\partial \theta}{\partial t} - \left[\frac{\partial \theta}{\partial t} \right]_{t=0^-} \right)$), energy exchanges by conduction ($k \Delta_2 \theta$) and energy exchanges by convection and radiation ($\rho C \left(\frac{\theta}{\tau_{th}^{2D}} \right)$). τ_{th}^{2D} is here a time constant characterizing the convection and radiation losses.

The dissipative and thermo-mechanical sources are coupled in Eq.(1)(thermo-mechanical coupling effects), although only the dissipative sources d_1 are of interest in this work. The loading signal was used to compute and remove the thermo-mechanical sources S_{th} and associated temperature variations from Eq.(1). As a result, dissipative sources d_1 were obtained. Eq.(1) was also integrated over the observed area Ω_{sp} and Ω_{dum} to lower the measurement noise level.

In this work, the mean dissipative sources were defined as $\bar{\bar{d}}_1$ to underline the spatial averaging. The spatial average $\bar{\bar{d}}_1$ is supposed to be representative of the dissipative sources field over the area Ω_{sp} . This hypothesis has been validated by computing the fields of dissipative sources d_1 using the method described in [9]. Eventually, the dissipated energy per cycle $E_{d_1}^i$ was computed by integrating $\bar{\bar{d}}_1$ over each cycle:

$$E_{d_1}^i = \int_{t_i}^{t_i+1/f} \bar{\bar{d}}_1 dt \quad (2)$$

Where t_i is the starting time of cycle i .

As the dissipated energy measurement is achieved in the elastic hysteretic domain, the dissipated energy should be constant during the test (15s). This characteristic was used a posteriori to check whether the test was performed in the elastic domain. The mean of the dissipated energy per cycle $E_{d_1}^m$ was thus computed over a time $t_m=12s$ to lower the noise level (Fig.4):

$$E_{d_1}^m = \frac{1}{t_m} \int_{t_0}^{t_0+t_m/f} E_{d_1}^i dt \quad (3)$$

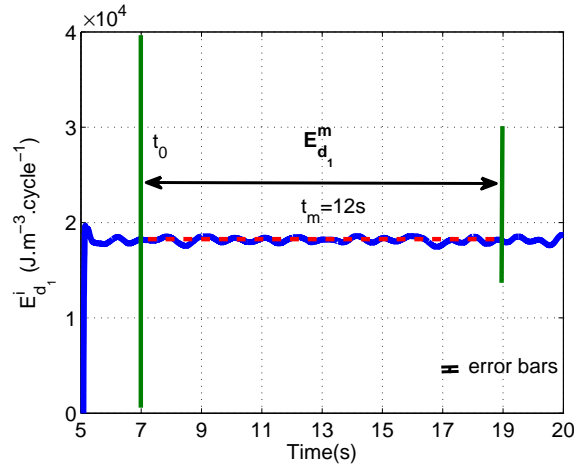


Figure 4: Definition of the mean dissipated energy per cycle $E_{d_1}^m$ (316L specimen).

The dissipated energy measurements have proved to be a reliable method[12]. With this method, the detection threshold of $E_{d_1}^m$ is as small as $\pm 222 J \cdot m^{-3} \cdot cycle^{-1}$ ($2\sigma_{E_{d_1}^m}$) for a 316L stainless steel specimen.

3. Results and discussion

It's known that in high fatigue test, damage is created slowly by dislocation pile-ups due to the small and gradual changes in the material microstructure. A test sequence was proposed to observe dissipated energy variation during the high cycle fatigue process, to better underline the in-situ thermo-mechanical modifications of materials. Serval specimens were loaded from $\sigma_{max}=280\text{MPa}$ to 440MPa in steps of 20MPa with $R_\sigma=0.2$ and $f=14\text{Hz}$.

Different constant amplitude fatigue tests (13 levels,30 specimens) were run until the specimen complete separation under traction-traction loadings (Tab.2). In each fatigue test, serval dissipated energy measurements were performed every 5,000, 10,000 or 30,000 cycles for different stress levels fatigue tests.

Table 2: Fatigue test results of 316L stainless steel ($R_\sigma=0.2, f=14\text{Hz}$)

Specimen number	σ_{max} (MPa)	σ_m (MPa)	σ_a (MPa)	N_f to failure	E_{d1}^m at 30,000 cycles ($J \cdot m^{-3} \cdot cycle^{-1}$)	Results
1	440	264	176	64,300	40,633	Failure
2	420	252	168	72,897	36,842	Failure
3	420	252	168	76,087	38,425	Failure
4	400	240	160	91,580	34,568	Failure
5	400	240	160	105,348	34,183	Failure
6	390	236	156	127,456	–	Failure
7	380	228	152	145,770	–	Failure
8	380	228	152	146,425	28,712	Failure
9	380	228	152	149,296	25,245	Failure
10	375	225	150	172,776	20,792	Failure
11	375	225	150	184,285	19,982	Failure
12	370	222	148	178,784	19,875	Failure
13	350	210	140	164,713	19,178	Failure
14	350	210	140	245,817	18,303	Failure
15	320	192	128	291,264	9,532	Failure
16	320	192	128	277,642	10,475	Failure
17	310	186	124	305,381	8,502	Failure
18	310	186	124	663,809	6,006	Failure
19	310	186	124	719,016	6,882	Failure
20	310	186	124	345,773	–	Failure
21	310	186	124	581,912	6,917	Failure
22	310	186	124	503,891	7,582	Failure
23	310	186	124	513,625	7,690	Failure
24	310	186	124	465,469	6,560	Failure
25	310	186	124	551,751	6,940	Failure
26	310	186	124	482,605	7,429	Failure
27	300	180	120	696,100	6,559	Failure
28	300	180	120	1,200,000	4,773	No Failure
29	290	174	116	2,000,000	4,317	No Failure
30	280	168	112	2,000,000	3,499	No Failure

Fig.5 and Fig.6 are dissipated energy variations in term of fatigue cycles ratio at different stress levels from

420MPa to 280MPa during fatigue test process, where N is the loading cycle, N_f is the cycles to failure (i.e. fatigue lifetime) and N/N_f represents fatigue loading cycles ratio. Dissipated energy per cycle E_{d1}^m was almost constant after 10% of total fatigue lifetime ($N/N_f=0.10$) beyond $\sigma_{max}=370\text{MPa}$) and 5% of total fatigue lifetime ($N/N_f=0.05$ in below $\sigma_{max}=350\text{MPa}$).

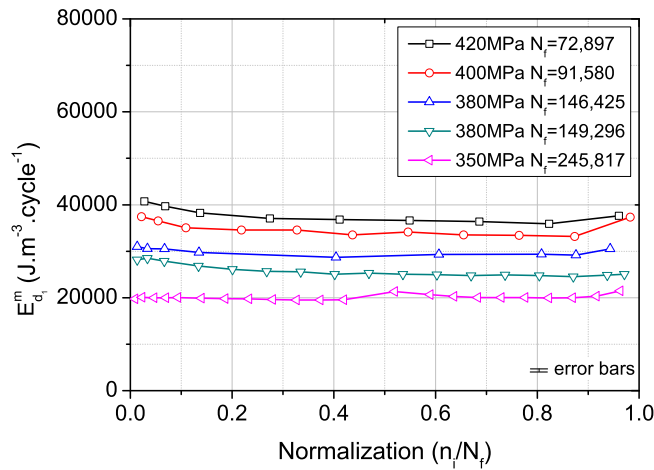


Figure 5: Dissipated energy variation during high cycle fatigue tests from 420MPa to 350MPa ($R_\sigma=0.2$, $f=14\text{Hz}$).

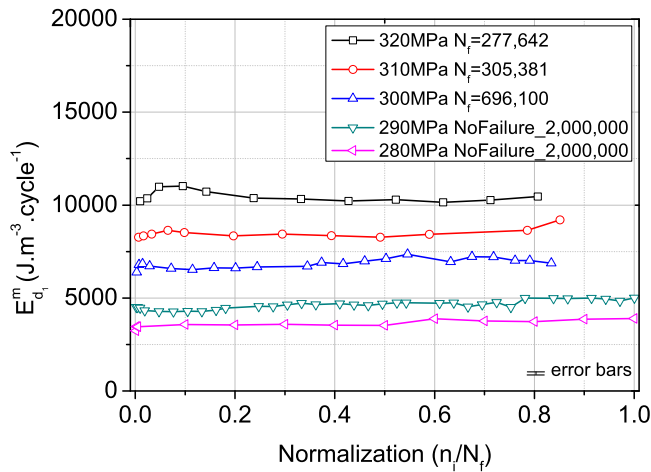


Figure 6: Dissipated energy variation during high cycle fatigue tests from 330MPa to 280MPa ($R_\sigma=0.2$, $f=14\text{Hz}$).

The same phenomenon about dissipated energy variation were observed by *Meneghetti, G* [8, 13]. In his method, the fatigue test must suddenly stop many time to measure the cooling curves to calculate the specific heat loss Q . The

measured values of Q for each specimen were within 15% with respect to the mean value. Thanks to the precise experiment set-up, the dissipated energy per cycle E_{d1}^m are with 5% of the mean value in these fatigue tests.

The constant stress amplitude fatigue tests (12 stress levels, 30 specimens in Tab.2) were performed to obtain the S-N curve by the traditional procedure (Fig.7). Meanwhile, Fig.8 shows that the relationship between the dissipated energy E_{d1}^m and fatigue lifetime N_f is very similar to the S-N curve. This curve was defined as E_{d1}^m -N curve in this work. The scatter bands of the two curves are given for 10% and 90% survival probability.

The linear fitting equation of E_{d1}^m -N curve is written as,

$$\log(E_{d1}^m) = -0.77\log(N_f) + 8.33 \quad (4)$$

where the related coefficient $R_{E_{d1}^m-N}^2$ between E_{d1}^m and N_f equals to 0.94.

The linear fitting equation of S-N curve is written as,

$$\log(\sigma_a) = -0.13\log(N_f) + 2.85 \quad (5)$$

where the related coefficient R_{S-N}^2 between σ_a and N_f equals to 0.89.

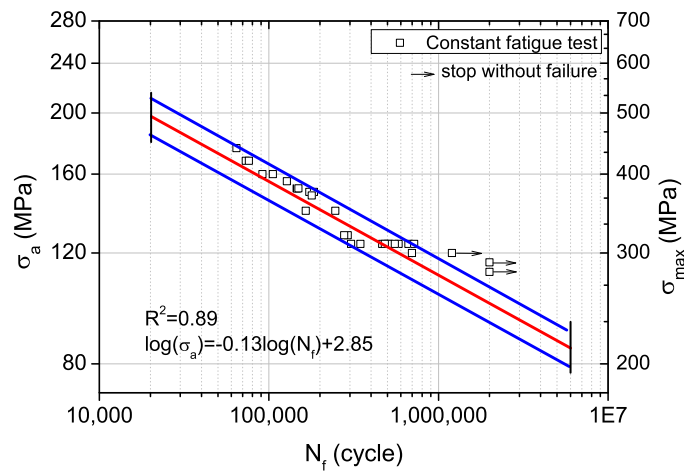


Figure 7: S-N curve by traditional staircase procedure of 316L material ($R_\sigma=0.2$, $f=14\text{Hz}$).

As $R_{E_{d1}^m-N}^2 > R_{S-N}^2$, E_{d1}^m -N curve by dissipated energy measurements shows more accurately than S-N curve by traditional fatigue test method. In such a case, it's possible to extrapolate the E_{d1}^m -N curve by dissipated energy measurements to predict the residual fatigue lifetime during various stress amplitude fatigue test under traction-traction cyclic loadings (i.e. $R_\sigma=0.2$).

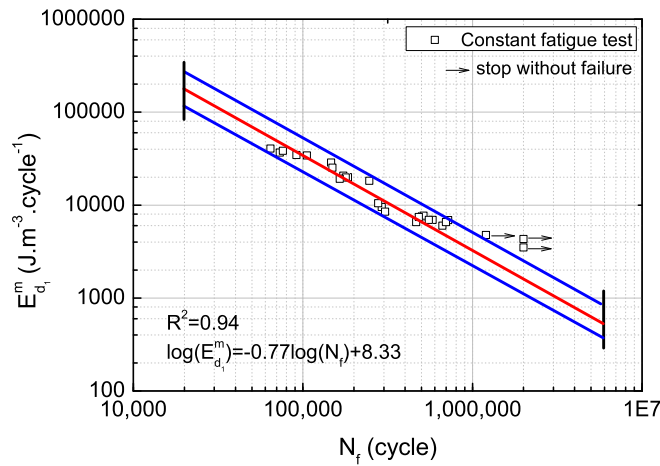


Figure 8: $E_{d_1}^m$ -N curve by dissipated energy $E_{d_1}^m$ method of 316L material ($R_\sigma=0.2$, $f=14\text{Hz}$).

4. Conclusion

In conclusion, dissipated energy per cycle $E_{d_1}^m$ is constant under traction-traction cyclic loadings during constant and various stress amplitude high cycle fatigue tests of 316L stainless steel while the material reached a stabilized thermo-mechanical state (5% of total fatigue lifetime). Dissipated energy versus fatigue lifetime fitting curve shows the same pattern as the traditional stress versus fatigue lifetime curve. Further studies and specific microstructural analysis are still required to better understand the correlation between the dissipated energy and the microstructural material state.

Acknowledgements

The work is partially supported by CSC(visiting scholarship) and NSFC(51175160). And I also especially acknowledge the supervision of Prof. Fabrice PIERRON and Dr. Francois MAQUIN in LMPF, ENSAM in France.

References

- [1] C. Mareau, V. Favier, B. Weber, A. Galtier, and M. Berveiller. Micromechanical modeling of the interactions between the microstructure and the dissipative deformation mechanisms in steels under cyclic loading. *International Journal of Plasticity*, 2012.
- [2] G. Fargione, A. L. Geraci, G. La Rosa, and A. Risitano. Rapid determination of the fatigue curve by the thermographic method. *International Journal of Fatigue*, 24(1):11–19, 2002.
- [3] M. P. Luong. Fatigue limit evaluation of metals using an infrared thermographic technique. *Mechanics of Materials*, 28(1-4):155–163, 1998.
- [4] M. Amiri and M. M. Khonsari. Life prediction of metals undergoing fatigue load based on temperature evolution. *Materials Science and Engineering A*, 527(6):1555–1559, 2010.
- [5] X. G. Wang, V. Crupi, X. L. Guo, and Y. G. Zhao. Quantitative thermographic methodology for fatigue assessment and stress measurement. *International Journal of Fatigue*, 32(12):1970–1976, 2010.
- [6] C. Doudard, S. Calloch, P. Cugy, A. Galtier, and F. Hild. A probabilistic two-scale model for high-cycle fatigue life predictions. *Fatigue and Fracture of Engineering Materials and Structures*, 28(3):279–288, 2005.
- [7] T. Boulanger, A. Chrysochoos, C. Mabru, and A. Galtier. Calorimetric analysis of dissipative and thermoelastic effects associated with the fatigue behavior of steels. *International Journal of Fatigue*, 26(3):221–229, 2004.
- [8] G. Meneghetti and M. Ricotta. The use of the specific heat loss to analyse the low- and high-cycle fatigue behaviour of plain and notched specimens made of a stainless steel. *Engineering Fracture Mechanics*, 2011.
- [9] N. Connesson, F. Maquin, and F. Pierron. Experimental energy balance during the first cycles of cyclically loaded specimens under the conventional yield stress. *Experimental Mechanics*, 51(1):23–44, 2011.
- [10] J. P. Strizak and L. K. Mansur. The effect of mean stress on the fatigue behavior of 316 In stainless steel in air and mercury. *Journal of Nuclear Materials*, 318(SUPPL):151–156, 2003.
- [11] F. Maquin and F. Pierron. Heat dissipation measurements in low stress cyclic loading of metallic materials: From internal friction to microplasticity. *Mechanics of Materials*, 41(8):928–942, 2009.
- [12] N. Connesson, F. Maquin, and F. Pierron. Dissipated energy measurements as a marker of microstructural evolution: 316l and dp600. *Acta Materialia*, 59(10):4100–4115, 2011.
- [13] G. Meneghetti. Analysis of the fatigue strength of a stainless steel based on the energy dissipation. *International Journal of Fatigue*, 29(1):81–94, 2007.